A CRISPR/Cas-Loaded Electronic Capsule Enables in vivo Nucleic Acid Monitoring in Gastrointestinal Tract

List:

Supplementary results

Supplementary methods

Supplementary figures: Figure S1-S15.

Supplementary tables: Table S1-S4.

Supplementary videos: Video S1-S5.

Supplementary results:

Primary optimization of dual-dCas9 system for target DNA detection

Two complexes of dCas9-LgBiT/sgRNA1 and dCas9-SmBiT/sgRNA simultaneously bind to the two adjacent regions in the same target DNA, bringing LgBiT and SmBiT protein fragments into proximity to reconstitute full NanoLuc enzyme activity. Firstly, using the Salmonella *invA* gene fragment as the detection target, we demonstrated through group settings with varying molecular additions that effective signals were produced only when both complexes bound to the target DNA simultaneously (Figures S6a, b). Subsequently, we optimized and determined that a 1:1 ratio of two protein complexes represented an optimal reaction condition (Figure S6c). In purified DNA template assays, the system achieved detection of as low as 10^{-3} nM target DNA fragments (Figure S6d). We then compared the one-step versus two-step detection modes and found that separating RPA amplification from CRISPR recognition significantly enhanced detection signals, yielding chemiluminescence intensities approximately 2-3 times higher than those of the one-step approach (Figures S6e-g). Therefore, the subsequent detection system adopted a two-step strategy. It was demonstrated that as low as 10^3 CFU/mL bacteria density could be significantly detected (Figure S6h).

Test of Bluetooth-based communication through porcine tissue in vitro

The capsule was designed to connect to mobile terminals via Bluetooth, enabling wireless control and data retrieval through a smartphone application (Figure S3d). To evaluate communication, we embedded the capsule in 10 cm-thick pork tissue to mimic the shielding effect of human tissue (Figure S4). Bluetooth signals were then measured at distances of 0, 15, 30, 45, and 60 cm from the capsule. The results showed a gradual decrease in signal intensity with increasing transmission distance, yet signals remained thoroughly

monitorable throughout, exhibiting a clear distance-dependent pattern (Figure S5a) and confirming that the wireless communication module met the requirements for in vivo data transmission.

Supplementary methods:

DNA degradation validation in simulated gastric fluid

To evaluate the degradation kinetics of DNA fragments in simulated gastric fluid, the linearized DNA or circular plasmids containing the *invA* gene were added to tubes containing simulated gastric fluid to final concentrations of 10 nM or 100 nM. The mixtures were gently mixed and incubated at 37 °C. Samples were withdrawn at 0, 0.5, 1, 2, and 3 h post-incubation and immediately placed on ice to terminate the enzymatic reaction. Residual invA gene fragments in the samples at each time point were quantified by qPCR. Each concentration group consisted of three parallel samples, and each qPCR reaction was performed in duplicate. The experiment was independently repeated three times, and results were expressed as mean ± SD.

Dual dCas9-sgRNA assay for nucleic acid detection

Guide RNAs (sgRNAs) targeting the *Salmonella invA* gene were designed using the online tool CRISPOR developed by Haeussler et al. The sequences are listed in Table S3 and were synthesized by Angsheng Life Science and Technology Co., Ltd. The synthesized sgRNA pellets were dissolved in IDTE (IDT nuclease-free duplex buffer) and stored for subsequent use. Pre-assembly of ribonucleoprotein (RNP) complexes was performed in a reaction mixture containing 2 μM dCas9-LgBiT-His or 2 μM dCas9-SmBiT-His protein, 7.5 μM sgRNA, and reaction buffer composed of 20 mM Tris-HCl (pH 7.5), 150 mM KCl, 5 mM $MgCl_2$, 5% (v/v) glycerol, 1 mM DTT, and 1 mg/mL BSA. The mixture was incubated at 37 °C for 20 min to form dCas9-Lg:gRNA1 and dCas9-Sm:gRNA2 RNP complexes, respectively, which were then stored at −80 °C until use. For detection, 5 μL of each RNP complex was added to a reaction buffer containing 20 mM Tris-HCl (pH 7.5), 150 mM KCl, 5 mM $MgCl_2$, 5% (v/v) glycerol, 1 mM DTT, and 1 mg/mL BSA to a final volume of 19 μL. Subsequently, 1 μL of the

target nucleic acid fragment was added, mixed thoroughly, and incubated at 37 °C for 30 min. After the reaction, signals were read using a microplate reader (VICTOR Nivo™, Revvity) for luminescence intensity, or chemiluminescence images were captured using an imaging system (Tanon-5200) for result interpretation.

Target DNA-dCas9-sgRNA binding validation

In a reaction buffer (20 mM Tris-HCl pH 7.5, 150 mM KCl, 5 mM $MgCl_2$, 5% (v/v) glycerol, 1 mM DTT, 1 mg/mL BSA), 50 nM of target or non-target DNA fragments were incubated with 0, 50, 200, or 800 nM of dCas9-Lg:gRNA1, dCas9-Sm:gRNA2, or both complexes combined, at room temperature for 1 h. Prior to electrophoresis, 6× loading buffer (BM111-01, TRANSGEN) was added to the reaction mixtures, and samples were loaded onto a 2% agarose gel. Electrophoresis was performed in TAE buffer (T1060, Solarbio) at a constant voltage of 150 V for 15 min. Bands were visualized and photographed using a chemiluminescence imaging system (UVITEC).

Quantitative PCR validation

Bacterial samples were lysed using either thermal lysis (98 °C for 10 min) or chemical lysis (5 mg/mL lysozyme (12650-88-3, HEOWNS), 20 mM Tris-HCl, 0.5 mM EDTA, 0.05% (V/V) NP40, 37 °C for 30 min). The lysates served as templates for amplification using SYBR Green master mix on a real-time PCR cycler (BIOER). Three groups were included: thermal lysis, paper-immobilized lysozyme, and non-lysed control. The reaction mixture (20 μL total) contained 10 μL SYBR Green master mix (Q132-03, Vazyme), 0.4 μM each of forward and reverse primers, and 1 μL template. The PCR program was as follows: initial denaturation at 95 °C for 30 s, followed by 40 cycles of 95 °C for 5 s and

60 °C for 30 s for annealing and extension. A melt curve analysis was performed post-amplification to verify product specificity. The non-lysed group served as the control, and lysis efficiency for each group was calculated using the comparative method. Each sample was run in triplicate to ensure data reliability.

Construction of *E. coli* MG1655 with *invA* integration

The λ-Red homologous recombination technique was employed to construct the gene knock-in recombinant fragment. Briefly, a partial sequence of the Salmonella invA gene was amplified by PCR, with its 5′ end fused to a 200 bp homology arm from the MG1655 lacZ gene, and its 3′ end linked to a chloramphenicol resistance gene (cat) flanked by FRT sites and another 200 bp homology arm from the MG1655 lacZ gene. These fragments were fused by overlap PCR, and the resulting linear recombinant DNA fragment was purified using a PCR product purification kit and stored at −20 °C until use.

The pKD46 plasmid (P54760, MiaoLing Biology) was introduced into MG1655 competent cells (ZC1040-1, ZOMANBIO) by chemical transformation, and the transformed cells were plated on LB agar plates containing 50 μg/mL kanamycin and incubated overnight at 30 °C. A single colony was picked and inoculated into 100 mL of LB liquid medium (supplemented with 50 μg/mL kanamycin and 10 mM L-arabinose) and cultured at 30 °C with shaking at 220 rpm to mid-log phase (OD_{600} ≈ 0.4–0.6). The culture was chilled on ice for 30 min, then centrifuged at 4,000 × g for 10 min at 4 °C. The supernatant was discarded, and the cell pellet was washed three to four times with pre-chilled 10% (v/v) glycerol. Finally, the cells were resuspended in an appropriate volume of 10% glycerol to prepare pKD46-MG1655 electrocompetent cells, which were aliquoted at 100 μL per tube and stored at −80 °C.

Approximately 1 μg of purified PCR-fused linear recombinant fragment was added to 100 μL of pKD46-MG1655 competent cells, gently mixed, and transferred to a pre-chilled electroporation cuvette (0.1 cm gap). Electroporation was performed using an electroporator (Bio-Rad) at 1,800 V, 200 Ω, and 25 μF. Immediately after electroporation, 1 mL of antibiotic-free LB liquid medium was added, gently mixed, and the cells were recovered at 30 °C with shaking at 220 rpm for 2 h. An appropriate volume of the recovered culture was plated on LB agar plates containing chloramphenicol (25 μg/mL) (C8050, Solarbio) and incubated at 30 °C for 24-48 h. Single colonies growing on the plates were picked and verified by colony PCR. The primers and related nucleic acid sequences are listed in Tables S3 and S4. PCR products were identified by agarose gel electrophoresis, and correctly sized amplicons were subjected to gene sequencing to confirm correct integration of the target gene fragment into the MG1655 genome.

Capsule sealing performance assessment

To evaluate the sealing performance and water absorption behavior of the encapsulated paper-based capsule in liquid environments, three fully assembled capsules were labeled #1, #2, and #3. The initial mass (m_0) of each capsule was recorded using an analytical balance. The capsules were individually immersed in 500 mL of PBS buffer (pH 7.4) in separate beakers, secured beneath floats to ensure complete submersion while avoiding contact with beaker walls or bottoms. The beakers were kept at room temperature (25 °C) under static conditions. At 2, 4, 6, and 24 h post-immersion, capsules were retrieved using clean forceps, surface moisture was gently blotted with filter paper, and the mass at each time point (m_t) was recorded before returning the capsules to the buffer.

Supplementary figures:

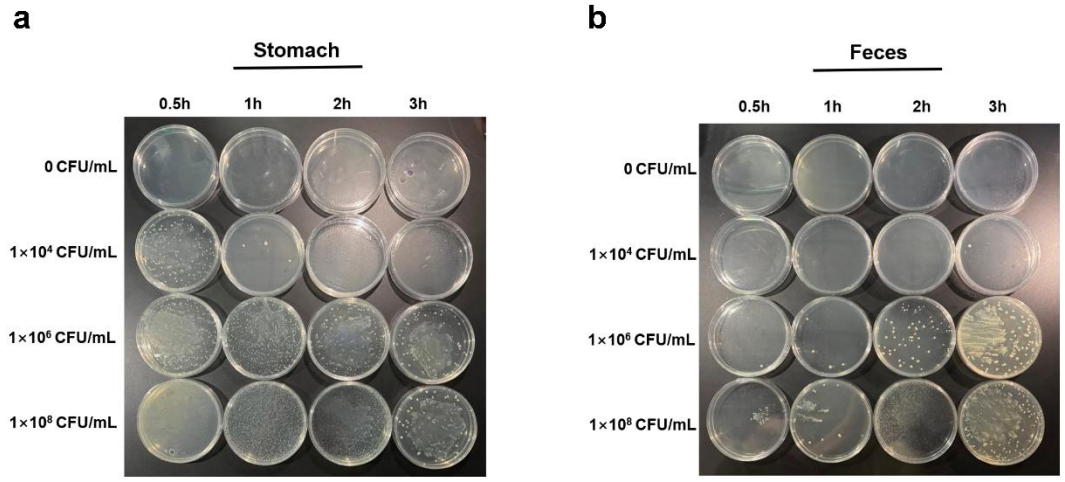


Figure S1. Temporal changes in viable bacterial loads in mice following oral gavage. a, Viable bacterial counts in mouse gastric tissues collected at different time points after oral gavage. **b**, Viable bacterial counts in mouse faecal samples collected at different time points after oral gavage.

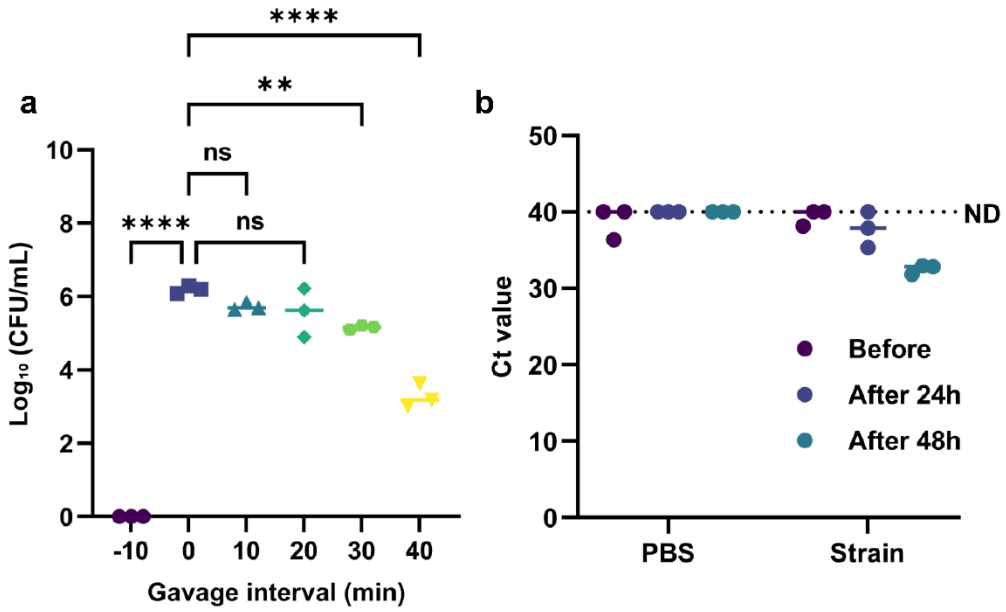


Figure S2. Temporal retention of pathogen signals in the gastric tract of pigs. a, qPCR analysis of pathogen loads in gastric fluid collected from pigs before oral gavage (−10 min) and at 0, 10, 20, 30 and 40 min after oral gavage. **b**, qPCR analysis of faecal samples collected from pigs before oral gavage and at 12 and 24 h after oral gavage, shown as Ct values.

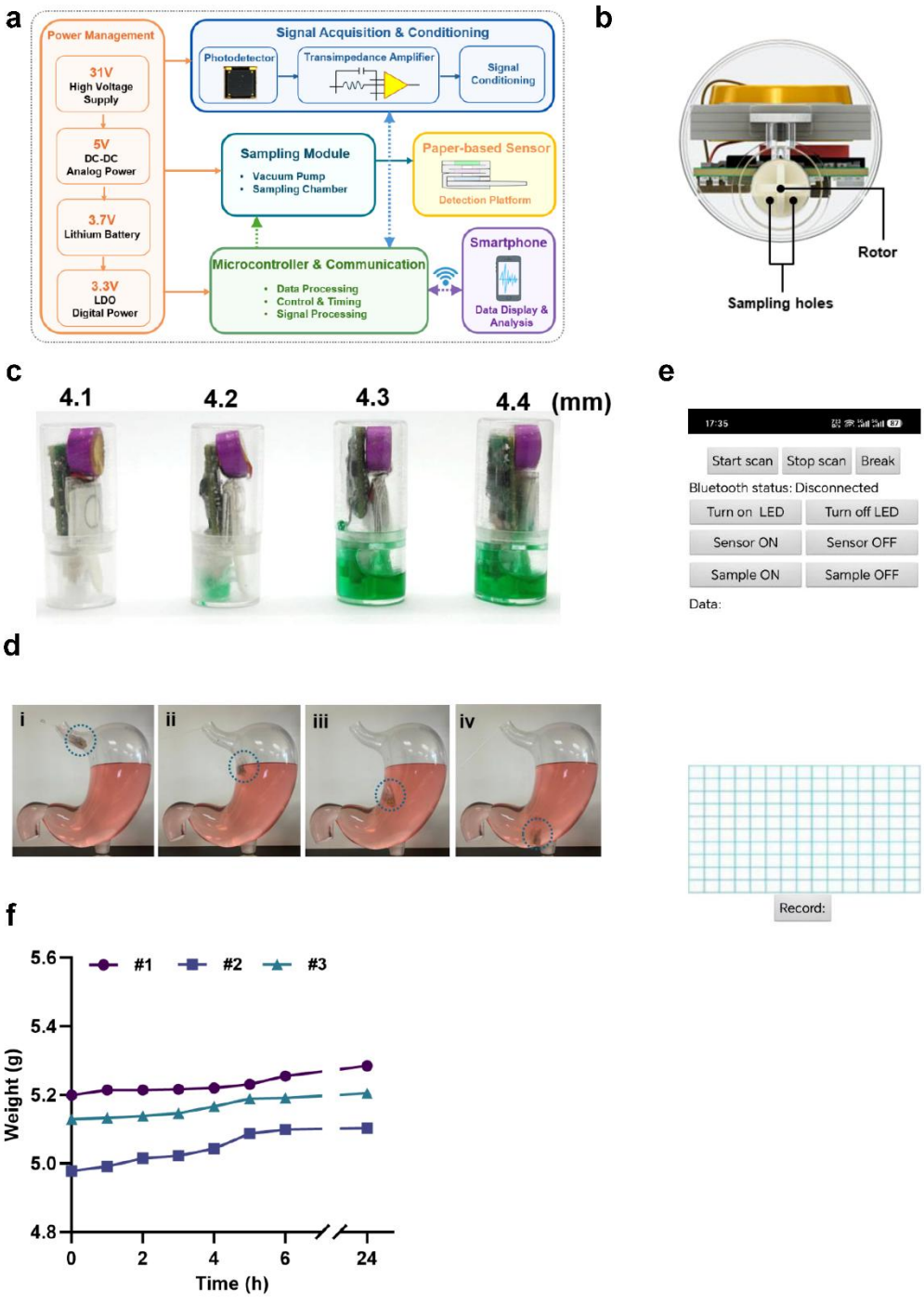


Figure S3. Optimization and characterization of the gastric sampling module. a, Block diagram of capsule electronic system. b, Three-dimensional schematic illustration of the electronic capsule from the sampling perspective. **c**, Photographs showing the sampling performance of the capsule with different impeller diameters in the sampling chamber. **d**, Sequential photographs illustrating the liquid sampling process of the capsule immersed in

a gastric model.**e**, Interface of the smartphone application for wireless operation and data readout. **f**, Changes in capsule mass (g) for capsules #1, #2 and #3 during immersion in liquid over 24 h.

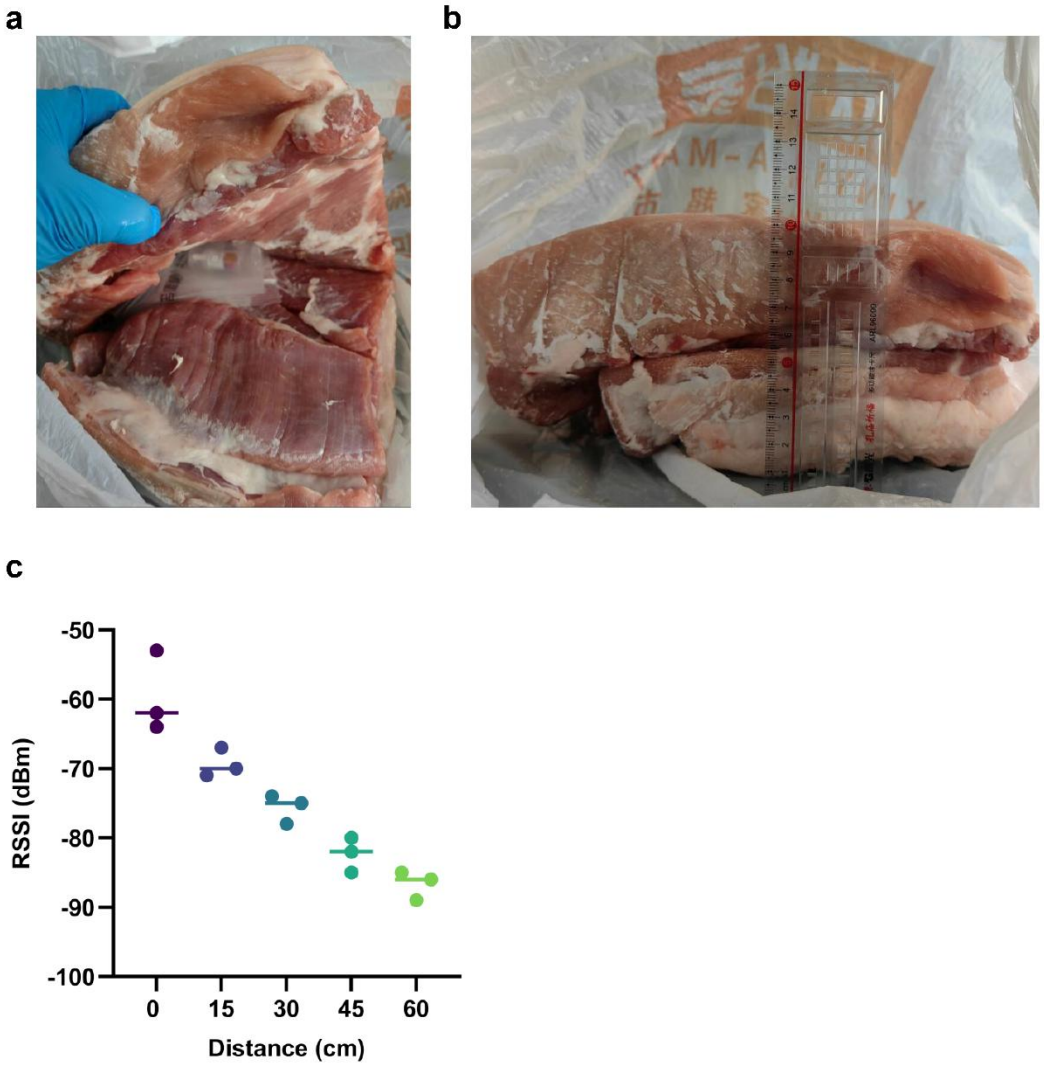


Figure S4. Wireless communication of the ingestible electronic capsule under tissue-mimicking conditions. a, Schematic illustration of the electronic capsule wrapped in pork tissue to simulate the in vivo environment for wireless Bluetooth signal evaluation. **b**, Measurement of the thickness of the pork tissue used for encapsulation. **c**, Bluetooth signal strength of the electronic capsule measured through pork tissue at different thicknesses (0, 15, 30, 45 and 60 cm).

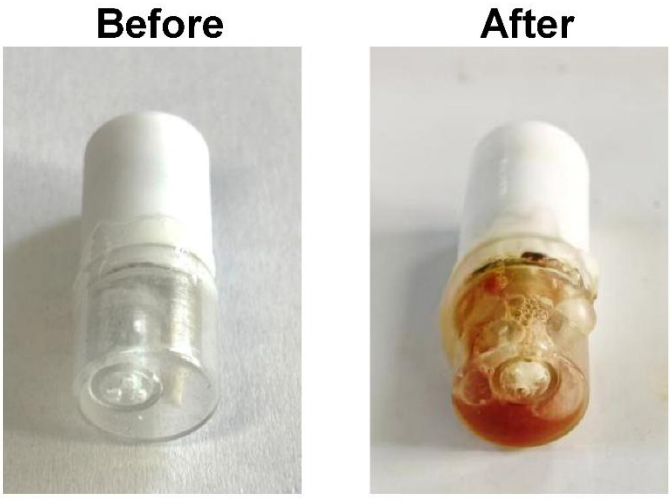


Figure S5. Validation of the ingestible capsule for sampling porcine gastric fluid. Photograph of the electronic capsule before (left) and after (right) gastric fluid sampling in a pig.

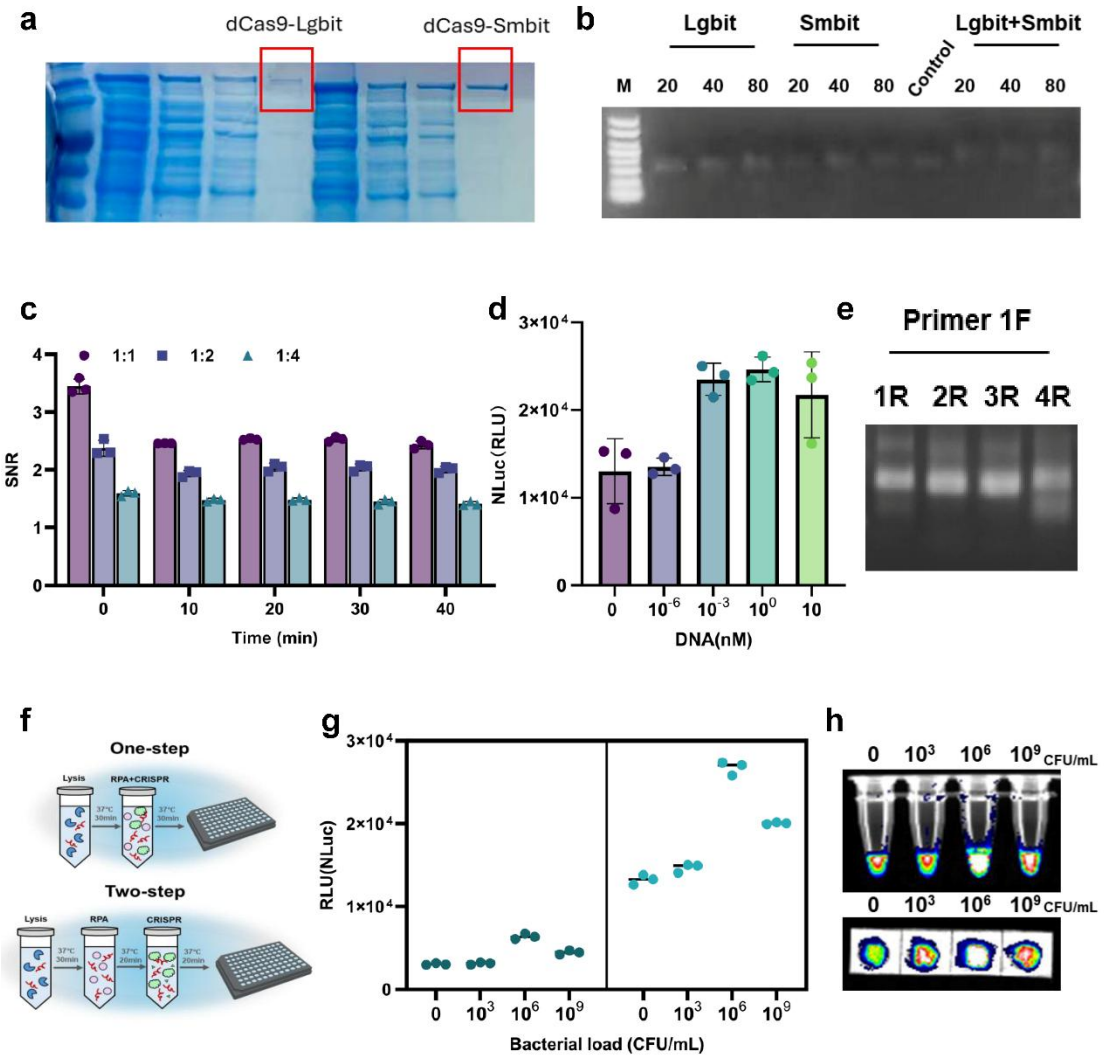


Figure S6. Development and optimization of the dCas9-based chemiluminescent nucleic acid detection system. a, SDS–PAGE analysis of purified dCas9-LgBiT and dCas9-SmBiT proteins. **b**, Agarose gel electrophoresis analysis of the binding of dCas9-LgBiT or dCas9-SmBiT to the target DNA fragment. **c**, Signal-to-noise ratios of the detection system at different dCas9-LgBiT/dCas9-SmBiT ratios. **d**, Concentration-dependent detection of target DNA fragments by the detection system at different reaction times. **e**, Agarose gel electrophoresis analysis of RPA products generated using different primer pairs. **f**, Schematic illustration of the one-step and two-step detection workflows in microplate-based assays. **g**, Comparison of fluorescence intensities obtained from the one-step and two-step detection

strategies at different bacterial loads. h, Representative chemiluminescence images of RPA–CRISPR reactions in tubes and on paper-based substrates.

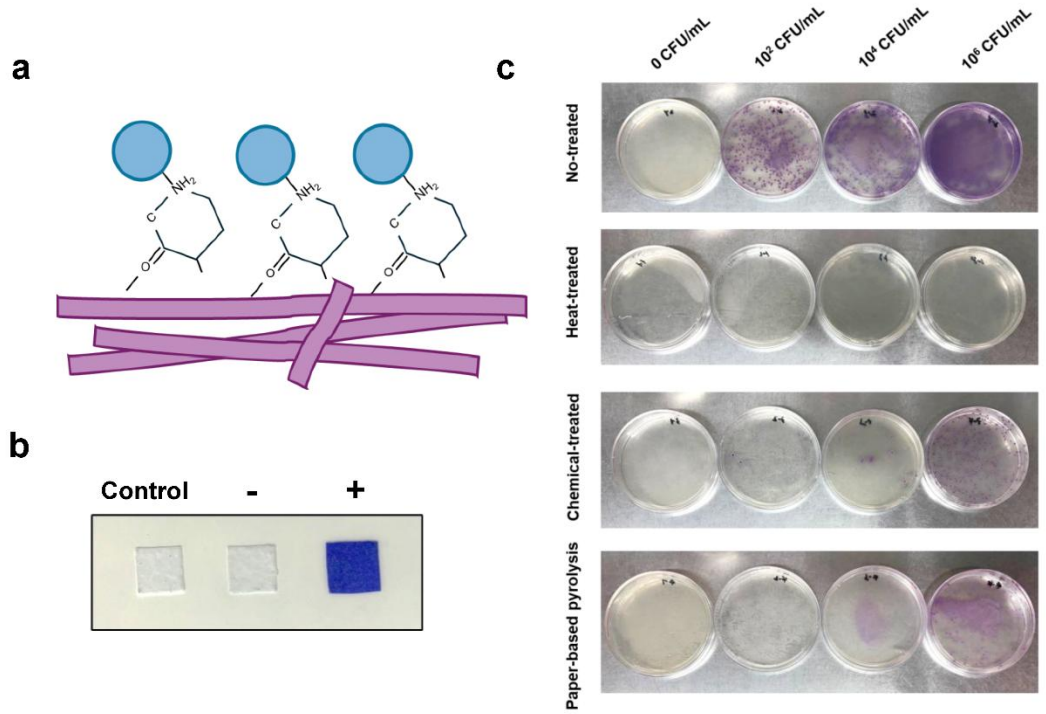


Figure S7. Development and characterization of the paper-based bacterial lysis module. **a**, Schematic illustration of lysozyme immobilization on Whatman filter paper. **b**, Photographs of paper-based substrates after Coomassie Brilliant Blue staining. The Control group underwent the immobilization procedure without lysozyme; the "–" group represents paper without immobilized lysozyme, whereas the "+" group represents paper with immobilized lysozyme. **c**, Photographs of bacterial colony growth after different bacterial loads of *Salmonella* were subjected to untreated, thermal lysis, chemical lysis or paper-based chemical lysis.

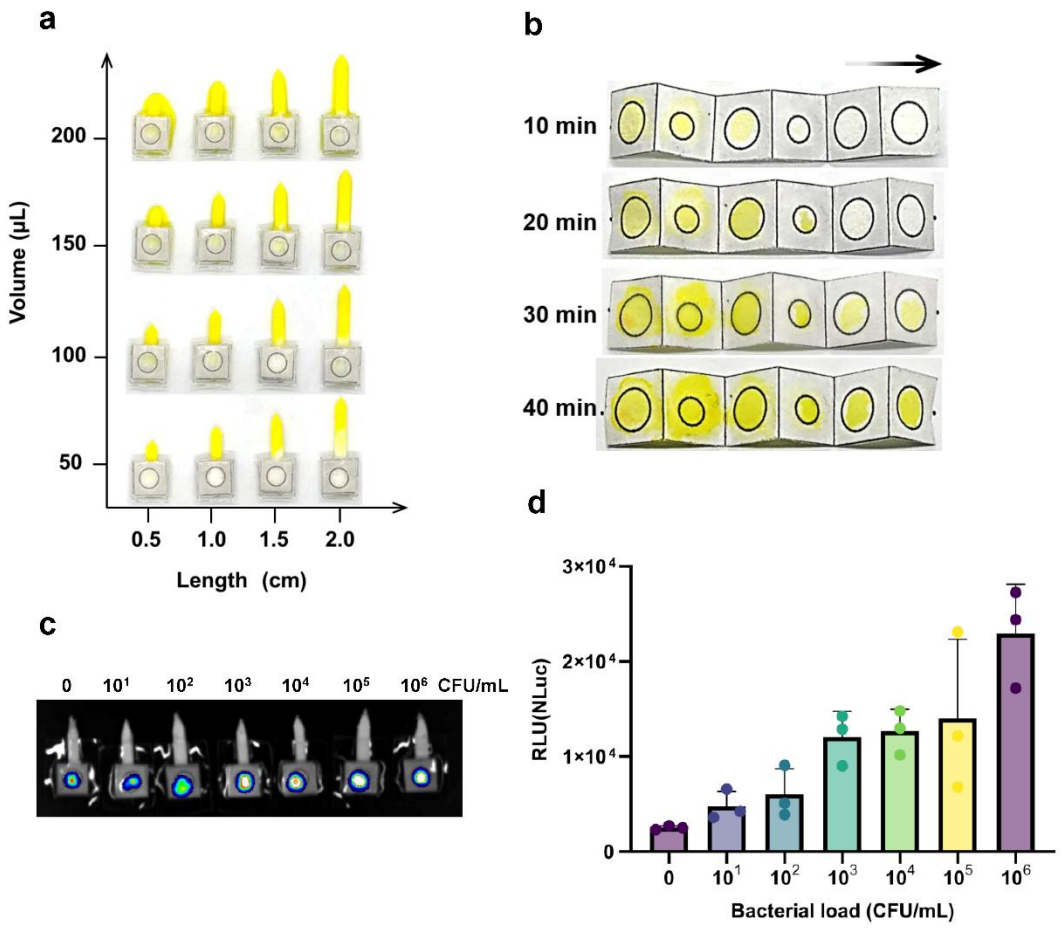


Figure S8. Optimization of fluid transport and analytical performance of the paper-based sensor. a, Relationship between the length of the absorbent strip and the liquid loading capacity of the paper-based sensor. **b**, Photographs showing the position of the liquid front within the paper-based sensor at different time points after sample loading. **c-d**, Chemiluminescence images and corresponding signal intensities of the paper-based sensor for the detection of different concentrations of *Salmonella*.

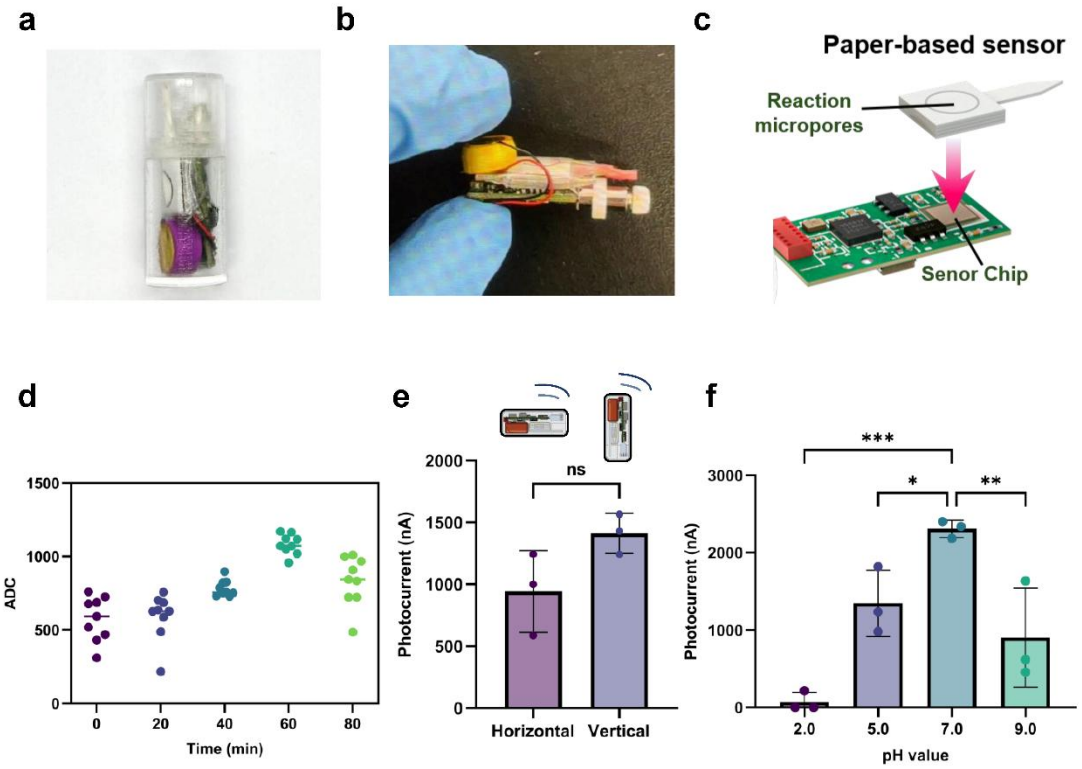


Figure S9. Electronic integration and operational stability of the ingestible electronic capsule. **a**, Photograph of the assembled ingestible electronic capsule. **b**, Photograph of the internal components of the electronic capsule. **c**, Three-dimensional schematic illustration of signal transduction between the paper-based sensor and the electronic circuit board. **d**, Photocurrent responses of the electronic capsule over a continuous detection period of 0, 20, 40, 60 and 80 min. **e**, Photocurrent responses of the electronic capsule positioned in horizontal and vertical orientations. **f**, Photocurrent responses of the electronic capsule under different pH conditions (pH 2.0, 5.0, 7.0 and 9.0).

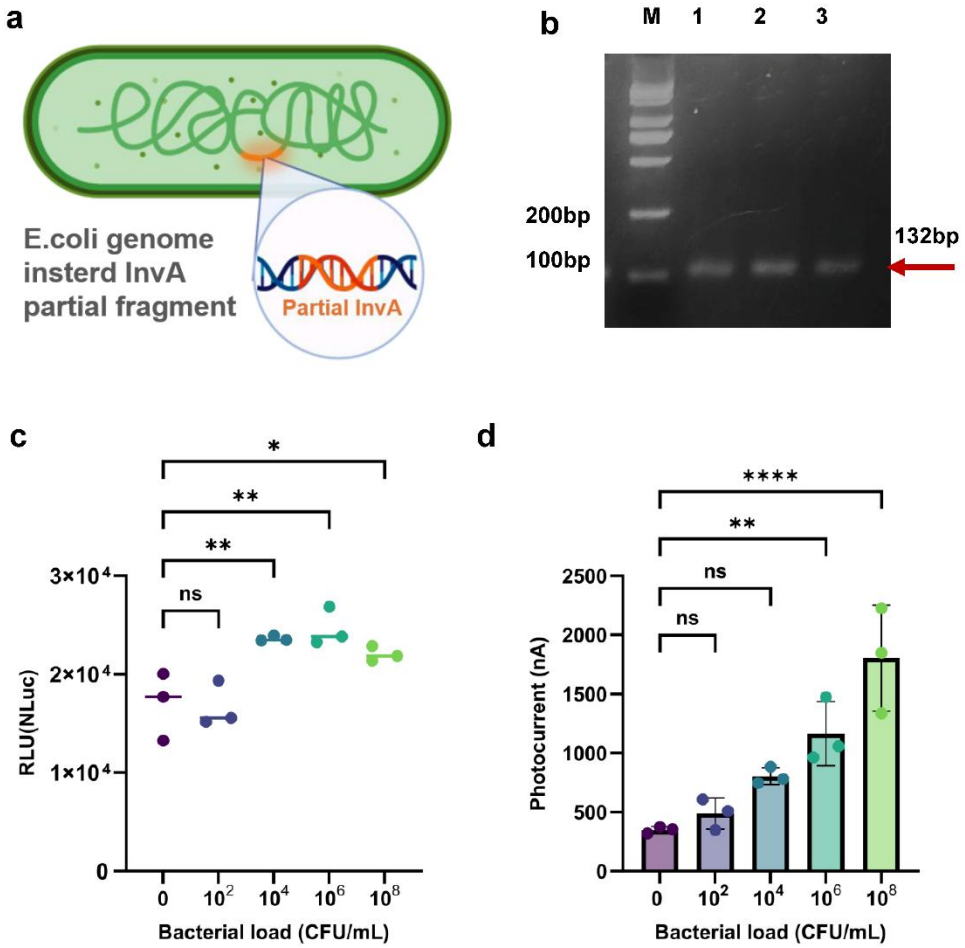


Figure S10. Construction and characterization of the MG1655 with *invA* (partial) for nucleic acid detection. **a**, Schematic illustration of the construction strategy for the MG1655 with *invA* (partial) strain. **b**, Agarose gel electrophoresis validation of the inserted InvA gene in the engineered strain. **c**, Fluorescence signals measured by a microplate reader for different bacterial loads of the InvA-integrated strain. **d**, Concentration-dependent photocurrent responses of the electronic capsule to the InvA-integrated MG1655 strain. Panel a created with BioRender.com

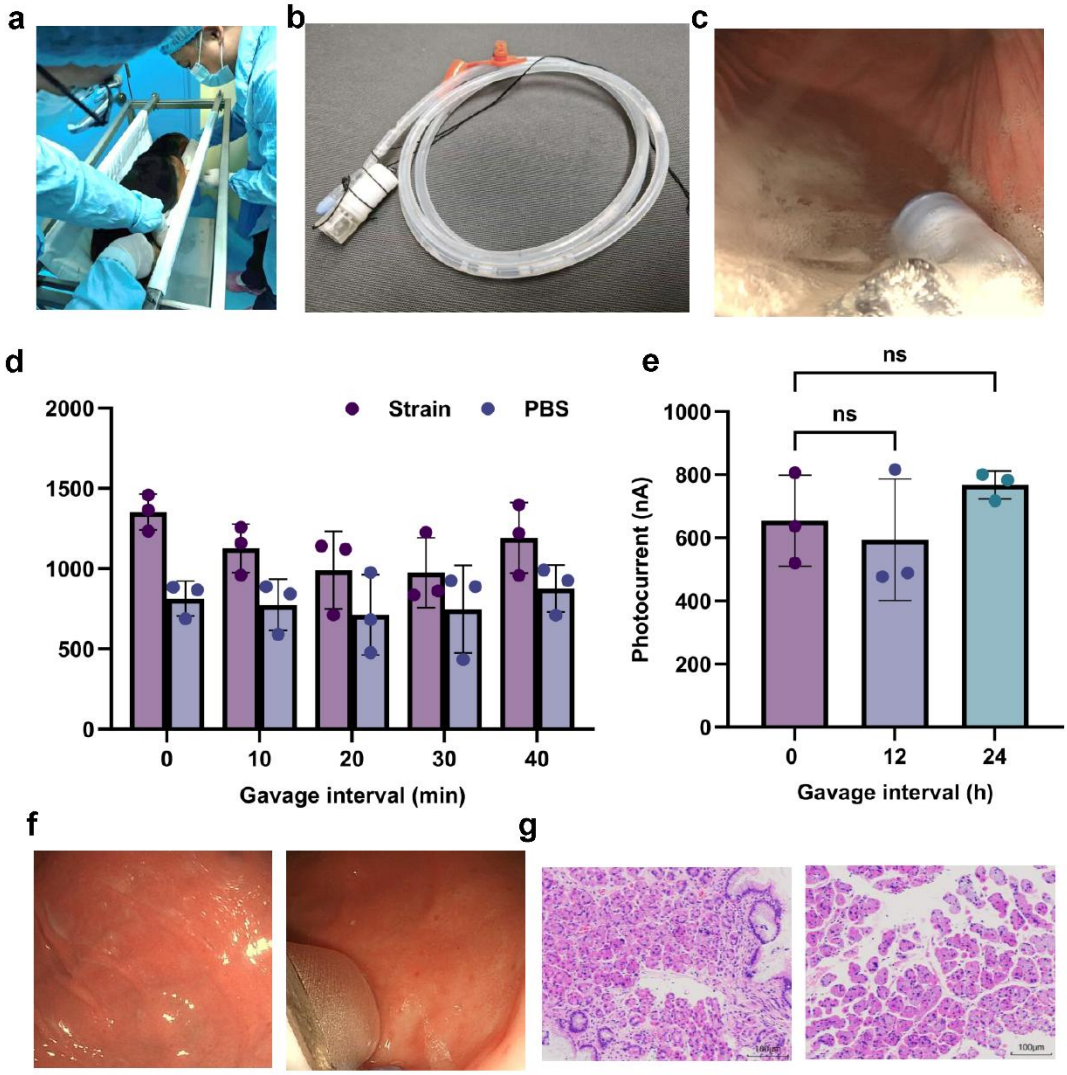


Figure S11. In vivo validation and histological assessment of the ingestible electronic capsule in dogs. **a**, Photographs showing the experimental procedures for canine model establishment and in vivo detection. **b**, Photograph of the electronic sensing capsule attached to a flexible tube. **c**, Endoscopic images showing in situ gastric sampling and detection with the electronic capsule. **d**, Photocurrent responses of the electronic capsule in the model and control (PBS) groups at 0, 10, 20, 30 and 40 min after oral gavage. **e**, Photocurrent responses of faecal samples collected before and at 12 and 24 h after oral gavage. **f**, Histological assessment of gastric tissues from dogs without capsule placement (left) and following capsule-based detection (right). **g**, Representative haematoxylin and eosin (H&E)-stained sections of canine

gastric tissues from dogs without capsule placement (left) and following capsule-based detection (right). Scale bar, 100 μm.

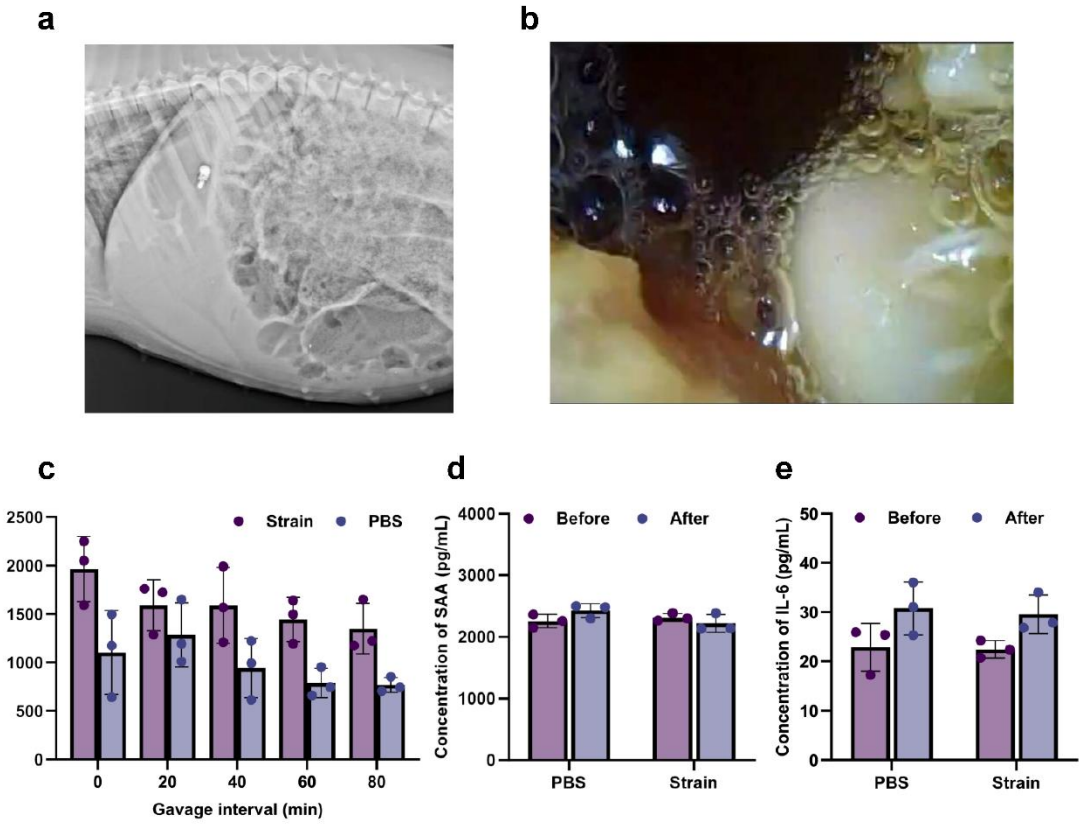


Figure S12. In vivo validation and biocompatibility assessment of the ingestible electronic capsule. a, X-ray image showing the electronic capsule positioned in the stomach of a pig for in situ detection. **b**, Endoscopic images showing the electronic capsule positioned in the porcine stomach. **c**, Comparison of photocurrent responses between the model and control groups (PBS) at 0, 20, 40, 60 and 80 min after oral administration. **d-e.** Serum levels of SSA (d) and IL-6 (e) measured by ELISA before and after placement of the electronic capsule.

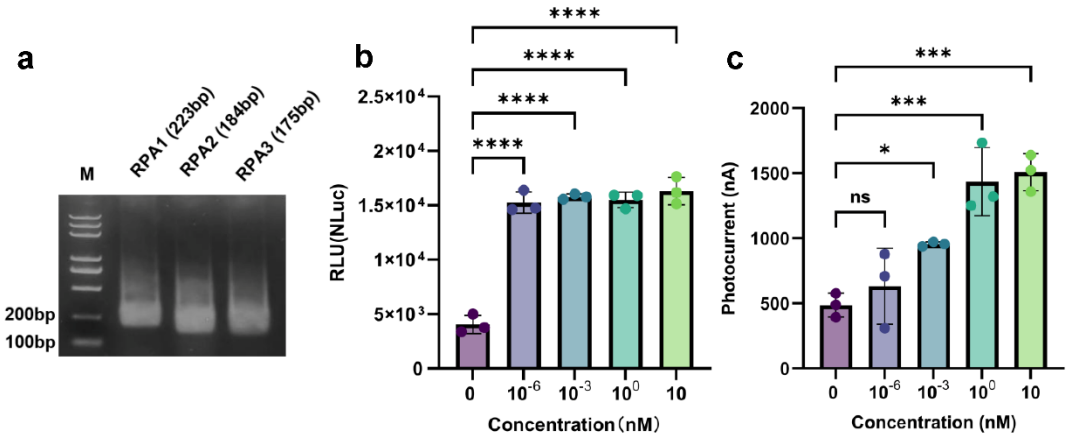


Figure S13. RPA amplification and CRISPR-based detection of the *Helicobacter pylori* 16S rRNA target. a, Agarose gel electrophoresis of RPA-amplified *H. pylori* 16S rRNA target sequences. **b-c**, Chemiluminescence responses (RLU) and photocurrent signals (nA) generated by the CRISPR-based detection of *H. pylori* 16S rRNA target sequences, respectively.

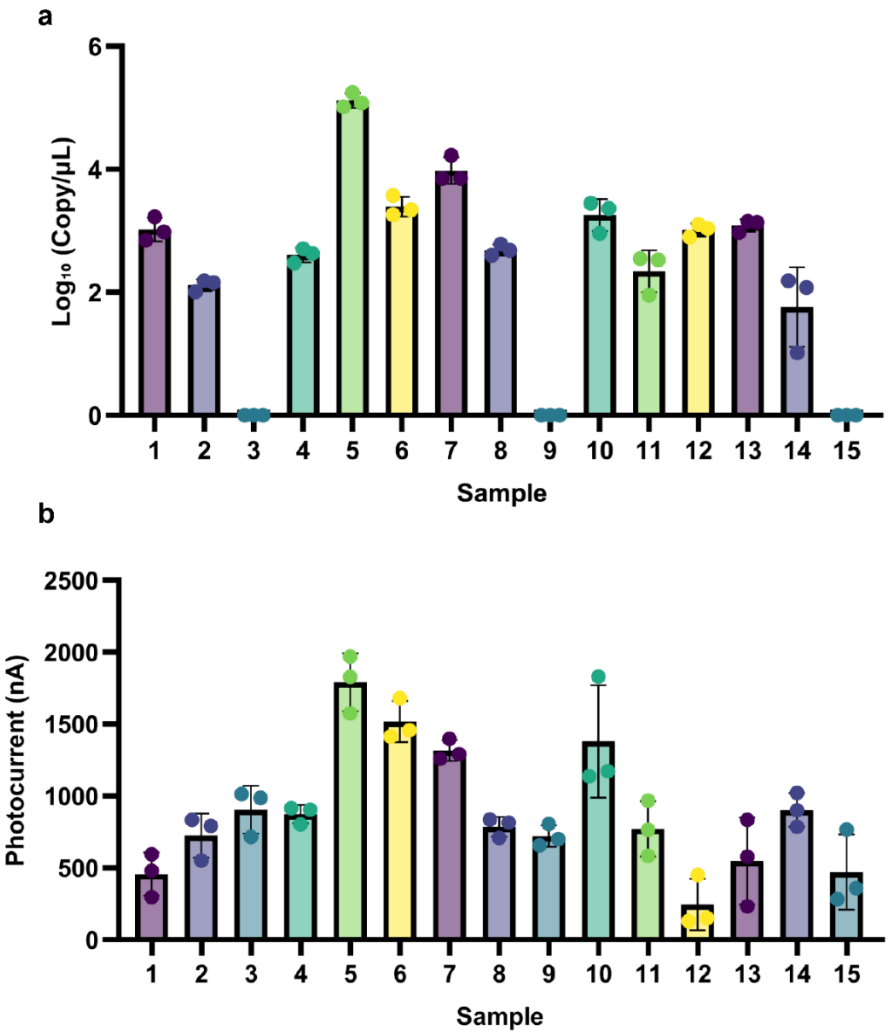


Figure S14. Molecular and electronic detection of Helicobacter pylori in clinical gastric fluid samples. a, Quantification of *Helicobacter pylori* nucleic acid copies in 15 clinical gastric fluid samples by qPCR. **b**, Photocurrent responses of the electronic capsule to the 15 clinical gastric fluid samples.

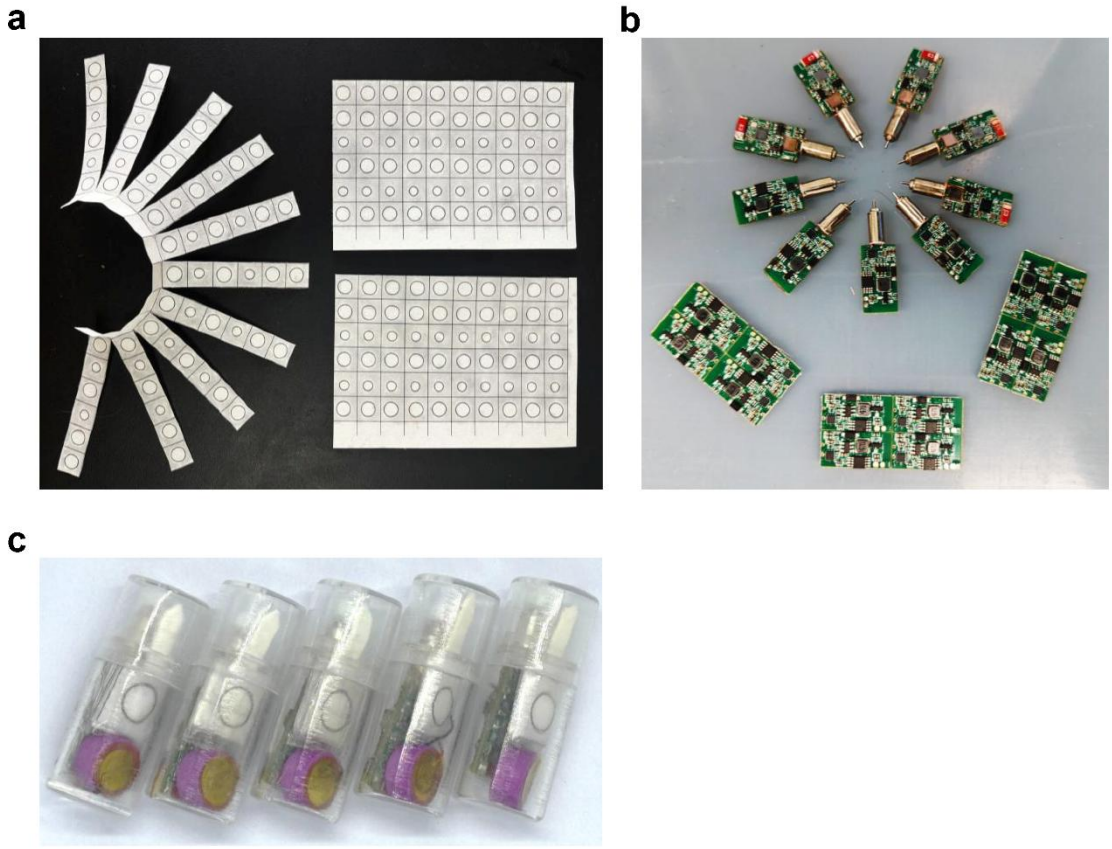


Figure S15. Scalable fabrication of the paper-based sensor and electronic capsule components. a, Design and batch fabrication of the paper-based sensors. **b**, Batch fabrication of the electronic circuit boards. **c**, Batch fabrication of the ingestible electronic capsules.

Supplementary tables:

Table S1. The constructed protein sequences.

Protein	Amino acid Sequence
dCas9-Smbit-6×His	MDKKYSIGLAIGTNSVGWAVITDEYKVPSKKFKVLGNTD RHSIKKNLIGALLFDSGETAEATRLKRTARRRYTRRKNRI CYLQEIFSNEMAKVDDSFFHRLEESFLVEEDKKHERHPI FGNIVDEVAYHEKYPTIYHLRKKLVDSTDKADLRLIYLAL AHMIKFRGHFLIEGDLNPDNSDVDKLFIQLVQTYNQLFE ENPINASGVDAKAILSARLSKSRRLENLIAQLPGEKKNG LFGNLIALSLGLTPNFKSNFDLAEDAKLQLSKDTYDDDL DNLLAQIGDQYADLFLAAKNLSDAILLSDILRVNTEITKAP LSASMIKRYDEHHQDLTLLKALVRQQLPEKYKEIFFDQS KNGYAGYIDGGASQEEFYKFIKPILEKMDGTEELLVKLN REDLLRKQRTFDNGSIPHQIHLGELHAILRRQEDFYPFL KDNREKIEKILTFRIPYYVGPLARGNSRFAWMTRKSEETI TPWNFEEVVDKGASAQSFIERMTNFDKNLPNEKVLPKH SLLYEYFTVYNELTKVKYVTEGMRKPAFLSGEQKKAIVD LLFKTNRKVTVKQLKEDYFKKIECFDSVEISGVEDRFNA SLGTYHDLLKIIKDKDFLDNEENEDILEDIVLTLTLFEDRE MIEERLKTYAHLFDDKVMKQLKRRRYTGWGRLSRKLIN GIRDKQSGKTILDFLKSDGFANRNFMQLIHDDSLTFKEDI QKAQVSGQGDSLHEHIANLAGSPAIKKGILQTVKVVDEL VKVMGRHKPENIVIEMARENQTTQKGQKNSRERMKRIE EGIKELGSQILKEHPVENTQLQNEKLYLYYLQNGRDMYV DQELDINRLSDYDVDAIVPQSFLKDDSIDNKVLTRSDKN RGKSDNVPSEEVVKKMKNYWRQLLNAKLITQRKFDNLT KAERGGLSELDKAGFIKRQLVETRQITKHVAQILDSRMN TKYDENDKLIREVKVITLKSKLVSDFRKDFQFYKVREINN YHHAHDAYLNAVVGTALIKKYPKLESEFVYGDYKVYDVR

	KMIAKSEQEIGKATAKYFFYSNIMNFFKTEITLANGEIRKR PLIETNGETGEIVWDKGRDFATVRKVLSMPQVNIVKKTE VQTGGFSKESILPKRNSDKLIARKKDWDPKKYGGFDSP TVAYSVLVVAKVEKGKSKKLKSVKELLGITIMERSSFEKN PIDFLEAKGYKEVKKDLIIKLPKYSLFELENGRKRMLASA GELQKGNELALPSKYVNFLYLASHYEKLKGSPEDNEQK QLFVEQHKHYLDEIIEQISEFSKRVILADANLDKVLSAYN KHRDKPIREQAENIIHLFTLTNLGAPAAFKYFDTTIDRKR YTSTKEVLDATLIHQSITGLYETRIDLSQLGGDTGGGSG GSGGSGGSGGSKLTSVTGYRLFEKESGGSHHHHHH*
dCas9-Lgbit-6×His	MDKKYSIGLAIGTNSVGWAVITDEYKVPSKKFKVLGNTD RHSIKKNLIGALLFDSGETAEATRLKRTARRRYTRRKNRI CYLQEIFSNEMAKVDDSFFHRLEESFLVEEDKKHERHPI FGNIVDEVAYHEKYPTIYHLRKKLVDSTDKADLRLIYLAL AHMIKFRGHFLIEGDLNPDNSDVDKLFIQLVQTYNQLFE ENPINASGVDAKAILSARLSKSRRLENLIAQLPGEKKNG LFGNLIALSLGLTPNFKSNFDLAEDAKLQLSKDTYDDDL DNLLAQIGDQYADLFLAAKNLSDAILLSDILRVNTEITKAP LSASMIKRYDEHHQDLTLLKALVRQQLPEKYKEIFFDQS KNGYAGYIDGGASQEEFYKFIKPILEKMDGTEELLVKLN REDLLRKQRTFDNGSIPHQIHLGELHAILRRQEDFYPFL KDNREKIEKILTFRIPYYVGPLARGNSRFAWMTRKSEETI TPWNFEEVVDKGASAQSFIERMTNFDKNLPNEKVLPKH SLLYEYFTVYNELTKVKYVTEGMRKPAFLSGEQKKAIVD LLFKTNRKVTVKQLKEDYFKKIECFDSVEISGVEDRFNA SLGTYHDLLKIIKDKDFLDNEENEDILEDIVLTLTLFEDRE MIEERLKTYAHLFDDKVMKQLKRRRYTGWGRLSRKLIN GIRDKQSGKTILDFLKSDGFANRNFMQLIHDDSLTFKEDI QKAQVSGQGDSLHEHIANLAGSPAIKKGILQTVKVVDEL

	VKVMGRHKPENIVIEMARENQTTQKGQKNSRERMKRIE EGIKELGSQILKEHPVENTQLQNEKLYLYYLQNGRDMYV DQELDINRLSDYDVDAIVPQSFLKDDSIDNKVLTRSDKN RGKSDNVPSEEVVKKMKNYWRQLLNAKLITQRKFDNLT KAERGGLSELDKAGFIKRQLVETRQITKHVAQILDSRMN TKYDENDKLIREVKVITLKSKLVSDFRKDFQFYKVREINN YHHAHDAYLNAVVGTALIKKYPKLESEFVYGDYKVYDVR KMIAKSEQEIGKATAKYFFYSNIMNFFKTEITLANGEIRKR PLIETNGETGEIVWDKGRDFATVRKVLSMPQVNIVKKTE VQTGGFSKESILPKRNSDKLIARKKDWDPKKYGGFDSP TVAYSVLVVAKVEKGKSKKLKSVKELLGITIMERSSFEKN PIDFLEAKGYKEVKKDLIIKLPKYSLFELENGRKRMLASA GELQKGNELALPSKYVNFLYLASHYEKLKGSPEDNEQK QLFVEQHKHYLDEIIEQISEFSKRVILADANLDKVLSAYN KHRDKPIREQAENIIHLFTLTNLGAPAAFKYFDTTIDRKR YTSTKEVLDATLIHQSITGLYETRIDLSQLGGDTGGGSG GSGGSGGSGGSKLTSVFTLEDFVGDWEQTAAYNLDQV LEQGGVSSLLQNLAVSVTPIQRIVRSGENALKIDIHIIPYE GLSADQMAQIEEVFKVVYPVDDHHFKVILPYGTLVIDGV TPNMLNYFGRPYEGIAVFDGKKITVTGTLWNGNKIIDER LITPDGSMLFRVTINSGGSHHHHHH*

Table S2. The primers used in this study.

Primer	Sequence (5′-3′)
InvA-F	GTGCTGCTTTCTCTACTTAACAGTGC
InvA-R	TTATATTGTTTTTATAACATTCACTG
LacZ-HR1-F	ATGACCATGATTACGGATTCACTG
LacZ-HR1-R	CAATACGATGCTGTTAGGTGCCGGAAACCAGG
InvA- Inserted -F	CCTGGTTTCCGGCACCTAACAGCATCGTATTG

InvA-Inserted-R	GAAGCAGCTCCAGCCTCCCTCTTCATGCGTTA
FRT-CM-FRT-F	TAACGCATGAAGAGGGAGGCTGGAGCTGCTTC
FRT-CM-FRT-R	GTGCGGTCGGCAAAGACCTTAGTTCCTATTCC
LacZ-HR2-F	AGAGAATAGGAACTTCGGAATAGGAACTAAGG
LacZ-HR2-R	AGCGACATCCAGAGGCACTTCACC
InvA-RPA-1/2/3-F	CCGTGTTGAACAATTTACGGTCTATTTTGAT
InvA-RPA-1-R	GCGTTACCCAGAAATACTGACTGCTACCTTG
InvA-RPA-2-R	GTTACCCAGAAATACTGACTGCTACCTTGCT
InvA-RPA-3-R	CTGCTACCTTGCTGATGGATTGTTGGATTAA
HP-RPA-1/3-F	CAAGGCTATGACGGGTATCCGGCCTGAGAGG
HP-RPA-2-F	TACCAAGGCTATGACGGGTATCCGGCCTGAG
HP-RPA-1-R	GGCACGGAGTTAGCCGGTGCTTATTCGTTAG
HP-RPA-2-R	ATCTTCTCTAACAAAAGGAGTTTACAATCCT
HP-RPA-3-R	TCTAACAAAAGGAGTTTACAATCCTAAAACC
InvA-qPCR -F	CGATGAAGTCGTGTCCTTTGGT
InvA-qPCR -R	CCTCTTCATGCGTTACCCAGAAA

Table S3. The SgRNA sequences used in this study.

SgRNA	Sequence (5′-3′)
InvA-SgRNA1	CUAUUUUGAUUUGAUGCGAGGUUUUAGAGCUAGAA AUAGCAAGUUAAAAUAAGGCUAGUCCGUUAUCAACU UGAAAAAGUGGCACCGAGUCGGUGCUUUU
InvA-SgRNA2	GAUUGUUGGAUUAAUACCAAGUUUUAGAGCUAGAA AUAGCAAGUUAAAAUAAGGCUAGUCCGUUAUCAACU UGAAAAAGUGGCACCGAGUCGGUGCUUUU
HP-SgRNA1	GUAGGGAAUAUUGCUCAAUGGUUUUAGAGCUAGAA AUAGCAAGUUAAAAUAAGGCUAGUCCGUUAUCAACU UGAAAAAGUGGCACCGAGUCGGUGCUUUU

HP-SgRNA2	UAAAACCUUCAUCCUCCACGGUUUUAGAGCUAGAA AUAGCAAGUUAAAAUAAGGCUAGUCCGUUAUCAACU UGAAAAAGUGGCACCGAGUCGGUGCUUUU

Table S4. The sequences related to construction of *E. coli* strain MG1655-InvA

Gene	Sequence (5′-3′)
Insertrd InvA (partial)	TAACAGCATCGTATTGTTGATTAATGAGATCCGTGTTG AACAATTTACGGTCTATTTTGATTTGATGCGAGTGGTA AATTATTCCGATGAAGTCGTGTCCTTTGGTATTAATCC AACAATCCATCAGCAAGGTAGCAGTCAGTATTTCTGG GTAACGCATGAAGAGGG
FRT-CM-cat promoter-FRT	GAAGTTCCTATACTTTCTAGAGAATAGGAACTTCGGAA TAGGAACTTCATTTAAATGGCGCGCCTTACGCCCCGC CCTGCCACTCATCGCAGTACTGTTGTAATTCATTAAGC ATTCTGCCGACATGGAAGCCATCACAAACGGCATGAT GAACCTGAATCGCCAGCGGCATCAGCACCTTGTCGC CTTGCGTATAATATTTGCCCATGGTGAAAACGGGGGC GAAGAAGTTGTCCATATTGGCCACGTTTAAATCAAAAC TGGTGAAACTCACCCAGGGATTGGCTGAGACGAAAA ACATATTCTCAATAAACCCTTTAGGGAAATAGGCCAGG TTTTCACCGTAACACGCCACATCTTGCGAATATATGTG TAGAAACTGCCGGAAATCGTCGTGGTATTCACTCCAG AGCGATGAAAACGTTTCAGTTTGCTCATGGAAAACGG TGTAACAAGGGTGAACACTATCCCATATCACCAGCTC ACCGTCTTTCATTGCCATACGTAATTCCGGATGAGCAT TCATCAGGCGGGCAAGAATGTGAATAAAGGCCGGATA AAACTTGTGCTTATTTTTCTTTACGGTCTTTAAAAAGG CCGTAATATCCAGCTGAACGGTCTGGTTATAGGTACAT TGAGCAACTGACTGAAATGCCTCAAAATGTTCTTTAC

	GATGCCATTGGGATATATCAACGGTGGTATATCCAGTG ATTTTTTTCTCCATTTTAGCTTCCTTAGCTCCTGAAAAT CTCGACAACTCAAAAAATACGCCCGGTAGTGATCTTAT TTCATTATGGTGAAAGTTGGAACCTCTTACGTGCCGAT CAACGTCTCATTTTCGCCAAAAGTTGGCCCAGGGCTT CCCGGTATCAACAGGGACACCAGGATTTATTTATTCTG CGAAGTGATCTTCCGTCACAGGTAGGCGCGCCGAAG TTCCTATACTTTCTAGAGAATAGGAACTTC

Supplementary videos:

Video S1. In vitro sampling by the electronic capsule.

Video S2. In vitro optical response of the electronic capsule.

Video S3. Endoscopic visualization of gastric sampling by the electronic capsule in a dog.

Video S4. Endoscopic visualization of gastric sampling by the electronic capsule in a pig.

Video S5. Tethered retrieval of the electronic capsule in a pig.